J Wood Sci (2012) 58:327–335
DOI 10.1007/s10086-012-1257-7

ORIGINAL ARTICLE

Moisture-induced stresses in engineered wood flooring with OSB substrate

Costel Barbuta · Pierre Blanchet · Alain Cloutier · Jean Deteix · André Fortin

Received: 28 October 2011 / Accepted: 22 February 2012 / Published online: 8 March 2012

Abstract Engineered wood flooring (EWF) is a multilayer composite flooring product. The cross layered structure is designed to give good dimensional stability to the EWF under changing environmental conditions. However, during winter season in North America, the indoor relative humidity could decrease dramatically and generate an important cupping deformation. The main objective of this study was to characterize the interlaminar stresses (σ_{33}, σ_{13} and σ_{23}) distribution at free-edges in EWF made with an OSB substrate. A three-dimensional (3D) finite element model was used to predict the cupping deformation and to characterize stresses developed in the EWF. The finite element model is based on an unsteady-state moisture transfer equation, a mechanical equilibrium equation and an elastic constitutive law. The physical and mechanical properties of OSB substrate were experimentally determined as a function of the density and moisture content. The simulated EWF deformations were compared against the laboratory observations. For both simulation and experimental results, the cupping deformation of EWF was induced by varying the ambient relative humidity from 50 to 20% at 20°C. A good agreement has been found between the numerical and experimental EWF cupping deformation. The stress distribution fields generated by the model correspond to the delaminations observed on the OSB substrate in the climate room. Delamination in EWF can occur principally under the action of the tension stress or a combination of tension and shear stresses. Finally, simulated results show that the levels of interlaminar stresses are maximal near the free-edges of EWF strips.

Keywords Layered structure · Delamination · Finite element analysis (FEA) · Wood testing

C. Barbuta (✉) · P. Blanchet
FPInnovations, 319 rue Franquet, Québec, QC G1P4R4, Canada
e-mail: costel.barbuta@fpinnovations.ca

A. Cloutier
Centre de recherche sur le bois, Université Laval,
Pavillon Gene-H.-Kruger, Québec, QC G1V0A6, Canada

J. Deteix · A. Fortin
Groupe interdisciplinaire de recherche en éléments finis (GIREF), Université Laval, Pavillon Alexandre-Vachon,
Québec, QC G1V0A6, Canada

Introduction

Engineered wood flooring (EWF) is a cross layered structure designed to give good dimensional stability under changing environmental conditions. However, during winter season in North America, the indoor relative humidity could decrease dramatically and generate an important cupping deformation. The magnitude of EWF deformation depends on the physical and mechanical properties of each layer and its behavior following changes in moisture content (MC) and temperature near the top surface.

Barbuta et al. [1] developed two types of OSB (Oriented Strand Board) as a substitute for Baltic Birch (*Betula pendula* Roth) plywood (BBP) used as a substrate for EWF. The specialty OSB panels were manufactured from two types of wood strands: a mixture of 90% aspen (*Populus tremuloides* Michx.) and 10% paper birch (*Betula papyrifera* Marsh.) and 100% ponderosa pine (*Pinus ponderosa* Dougl. ex Laws.). In a second study, Barbuta et al. [2] evaluated the performance of EWF prototypes manufactured with OSB substrate in conditioning room. They found that there was no significant difference, in terms of cupping deformation, between the EWF manufactured with

aspen/birch OSB and BBP substrate. However, after the evaluation test in conditioning room, delaminations were observed in the specialty OSB substrate. These delaminations are the result of the high level of interlaminar stresses distribution at free-edges in EWF.

The finite element method is a useful tool to predict the behavior of EWF [3, 4]. Blanchet et al. [5] developed a three-dimensional (3D) finite element model of the hygromechanical cupping in layered wood composite flooring. The model was based on two sets of equations: (1) the three-dimensional equations of unsteady-state moisture diffusion and (2) the three-dimensional equations of elasticity including the orthotropic Hooke's law which takes into account the shrinkage and swelling of each layer. Blanchet et al. [6] used this finite element model to support the design of EWF. They first demonstrated that at the macroscopic level, the hypothesis of elastic linearity is acceptable. Geometrical parameters and wood species properties were then used to assess different EWF construction. They found that the thickness and mechanical properties of the core layer are the most important design parameters controlling cupping deformation of EWF in service. They also indicated that the backing layer has a smaller, although still significant, impact on cupping.

The wood-adhesive interface was characterized by Belleville et al. [7] to determine its impact on EWF hygromechanical behavior. The finite element analysis has shown that better results are obtained when the wood-adhesive interface is considered in the model.

Deteix et al. [8] have investigated the impact of the adhesive layer on the dimensional stability of layered wood composites and how it should be modeled by the finite element method. They showed that the use of a finite element mesh with a single layer of elements in the adhesive layer can lead to significant errors. This is particularly true for low values of the adhesive effective diffusion coefficient.

The objectives of the current study are to determine the physical and mechanical properties of the OSB substrate and to characterize stresses leading to delamination at the free-edge of EWF with an OSB substrate by the finite element method.

Materials and methods

Physical and mechanical properties of EWF components

The mechanical and physical properties of OSB panels were experimentally determined in laboratory. Unidirectional OSB panels were manufactured with three target densities: 500, 650 and 800 kg/m^3. Flat density profiles through panel thickness were achieved using a temperature of 100°C during press closing. When the nominal thickness was reached, the platens temperature was raised until the core temperature achieved 140°C. The platen temperature corresponding to a core temperature of 140°C was 165°C. The other OSB manufacturing parameters were the same as those used by Barbuta et al. [1, 2] in the production of aspen/birch OSB panels. A total of 30 panels were manufactured. The physical and mechanical properties were determined for each density. The mechanical properties were also determined for two RH levels: 50 and 20% at 20°C. These two environmental conditions represent the initial and final stages of the numerical simulation. The properties determined were modulus of elasticity (E_L, E_T and E_R), shear modulus (G_{LR} and G_{TR}), interlaminar shear strength (S_{LR} and S_{TR}), internal bond strength (IB), shrinkage coefficients (β_L, β_T and β_R) and the diffusion coefficients (D_L, D_T and D_R). Tension and shear properties were determined using the ASTM D 1037[9] standard. The L, T and R directions correspond to the longitudinal, transverse and through-thickness directions of the unidirectional OSB panel. The modulus of elasticity perpendicular to the panel surface (E_R) was determined using a 5 mm MTS extensometer (Model 632.29F-30) attached to the test specimen. The shrinkage coefficients for each density between 50% RH and 20% RH were determined using Eq. 1:

$$\beta = \frac{d_{50} - d_{20}}{d_{50}\Delta M} \quad (1)$$

where d_{20} is the dimension at 20% RH (mm), d_{50} is the dimension at 50% RH (mm), and ΔM is the moisture content difference (%)

The steady-state method used to determine the diffusion coefficient was inspired from Siau [11]. Twenty-five diffusion cells were prepared for each density. The water vapor diffusion coefficients were determined by the following equation:

$$D = \frac{100wL}{tA\rho_w G\Delta M} \quad (2)$$

where w/t is the water vapor flow (kg s^{-1}), L is the length in the flow direction (m), A is the cross-section area of specimen normal to the flow direction (m^2), ρ_w is the water density (1000 kg m^{-3}), G is the specific gravity of wood at the average moisture content, and ΔM is the moisture content difference across specimen thickness (%)

To model the behavior of EWF, the physical and mechanical properties of all materials were needed. The properties of maple sugar layer, PVA adhesive type I and the six Poisson's ratios (v_{ij}) for OSB were also taken from the literature. The parameters used in the numerical model are presented in Table 1.

Finite element modeling

The EWF strip considered in this study is made of a 3-mm thick sugar maple surface layer and a 9-mm thick OSB substrate layer (Fig. 1). The OSB substrate is composed of three cross-oriented layers. The ratio between the two surface layers and the core layer is 0.45/0.1/0.45. The adhesive used to bond the surface layer and the substrate is a type I PVA (polyvinyl acetate). The thickness of the adhesive layer was estimated to be 0.1 mm [8]. The construction of EWF strips was designed such that the longitudinal axis of the substrate surface layers would be perpendicular to that of the sugar maple wood layer.

The cupping deformation was generated by varying relative humidity (RH) from 50 to 20% at 20°C. This corresponds to a decrease in moisture content from 8.6 to 5.8% for the sugar maple surface layer and PVA adhesive and from 6.2 to 3.4% for OSB substrate. The water vapor desorption occurred by free convection at the top of the surface layer. All the other surfaces were assumed impervious.

The theoretical model of hygromechanical EWF deformation used in this study is based on the model developed by Blanchet et al. [5] and improved by Deteix et al. [8] and Belleville et al. [7]. The governing equations used in the model are three-dimensional moisture conservation (3 and 4), three-dimensional equation of mechanical equilibrium (5) and Hooke's law for orthotropic materials which takes into account the shrinkage of each layer (6).

The moisture transfer is described by the equation:

$$\frac{d_b}{100}\frac{\partial M}{\partial t} + \vec{\nabla}\cdot\left(-\boldsymbol{K}_M\vec{\nabla}M\right) = 0 \quad \text{with } \boldsymbol{K}_M = \frac{\boldsymbol{D}d_b}{100} \tag{3}$$

where $\boldsymbol{K}_M$ is the tensor of effective water conductivity (kg m^{-1} s^{-1} %$^{-1}$), $\boldsymbol{D}$: tensor of effective moisture diffusion (m^2 s^{-1}), d_b is the basic density (kg m^{-3}), t is the time (s) and M is the moisture content (%).

The moisture transfer in EWF can be written in the following manner:

$$\frac{\partial M}{\partial t} - \left\{\frac{\partial}{\partial x_1}\frac{\partial}{\partial x_2}\frac{\partial}{\partial x_3}\right\}\left[\begin{pmatrix} D_{11} & 0 & 0 \\ 0 & D_{22} & 0 \\ 0 & 0 & D_{33}\end{pmatrix}\begin{Bmatrix}\frac{\partial M}{\partial x_1}\\ \frac{\partial M}{\partial x_2}\\ \frac{\partial M}{\partial x_3}\end{Bmatrix}\right] = 0 \tag{4}$$

The mechanical model is based on the three-dimensional equation of mechanical equilibrium:

$$\frac{\partial \sigma_{ij}}{\partial x_j} = 0 \quad i,j = 1,2,3 \tag{5}$$

where σ_{ij} is the normal and shear stress components (Pa).

It is assumed that the wood surface layer, the OSB substrate and the adhesive are elastic. The stress tensor is calculated using Hooke's law for the stress–strain relationship.

$$\sigma_{ij} = C_{ijkl}(\varepsilon_{kl} - \beta_{kl}\Delta M) \tag{6}$$

where $\boldsymbol{C}_{ijkl}$ is the stiffness tensor, ε_{kl} is the normal and shear strain components, β_{kl} is the moisture shrinkage coefficients (%$^{-1}$), and ΔM is the moisture content change between two time steps (%).

The normal and shear strains ε_{ij} and displacements u_i are related by the equation:

$$\varepsilon_{ij} = \frac{1}{2}\left(\frac{\partial u_i}{\partial x_j} + \frac{\partial u_j}{\partial x_i}\right) \tag{7}$$

The finite element (FE) modeling of hygromechanical deformation of EWF was performed using the FE code MEF++ developed by the GIREF (Interdisciplinary Research Group on Finite Elements) at Université Laval, Québec, Canada. The computational domain is a 50-mm length EWF strip (Fig. 2). This dimension corresponds to EWF sample length generally used in the delamination test. Two FE meshes corresponding to half of this domain were generated with increasing element densities. The relatively coarse and fine meshes contained 117900 and 495450 ten-node tetrahedral elements. The 0.1-mm thick adhesive layer was meshed with three layers of elements. Figures 3 and 4 illustrate the coarse and the fine meshes used in this numerical experiment.

Each layer of EWF is assumed to be elastic. It is also assumed that the principal material directions of the sugar maple surface layer and the three sublayers of the OSB substrate are perfectly oriented with the strip. The experimental data obtained for unidirectional OSB panels were linearly extrapolated to calculate the physical and mechanical properties of OSB substrate function of the vertical density profile (VDP) and the ΔM. For FE simulations, the initial moisture content M_0 was set at 8.6% for the sugar maple surface layer and PVA adhesive and 6.2% for OSB substrate. This was due to the different sorption isotherm of these two materials. The equilibrium moisture content M_∞ was as follows: 5.8% for surface layer and PVA adhesive and 3.4% for OSB substrate. It was assumed that moisture transfer occurs only through the top of the surface layer.

Boundary condition:

$$q = h(M - M_\infty) \quad \text{on exposed face} \tag{8}$$

$$q = 0 \quad \text{on the other surfaces} \tag{9}$$

where, q is the moisture flux (kg$_{water}$ m$^{-2}_{wet\ wood}$ s^{-1}), h is the convective mass transfer coefficient (kg m^{-2} s^{-1} %$^{-1}$), M is the moisture content (%), and M_∞ is the moisture content at equilibrium (%)

The initial condition for moisture content was:

Table 1 Finite element model parameters

Parameters	Material							
	Surface	Substrate						Adhesive
	Sugar maple	OSB						PVA I
d_b (kg/m^3)	597[a]							1178[i]
d_n (kg/m^3)		500[f]		650[f]		800[f]		4.18×10^{-12}[i]
D (m^2 s^{-1})								
D_L (m^2 s^{-1})	2.20×10^{-9}[b]	–		–		–		
D_T (m^2 s^{-1})	1.80×10^{-11}[c]	–		–		–		
D_R (m^2 s^{-1})	1.80×10^{-11}[c]	2.63×10^{-11}		1.33×10^{-11}[f]		6.68×10^{-12}[f]		
T (°C)		20[f]		20		20		
RH (%)		50	20	50	20	50	20	
D_R (m^2 s^{-1})	1.80×10^{-11}[c]	2.63×10^{-11}[f]		1.33×10^{-11}[f]		6.68×10^{-12}[f]		
M_0 (%)	8.6	6.2	–	6.2	–	6.2	–	8.6
M_1 (%)	5.8	–	3.4	–	3.4	–	3.4	5.8
h (kg m^{-2} s^{-1} %$^{-1}$)	3.20×10^{-4}[b]			3.20×10^{-4}[b]				3.20×10^{-4}[b]
								3×10^{-3}[i]
β (m m^{-1} %$^{-1}$)								
β_L (m m^{-1} %$^{-1}$)	1.50×10^{-4}[d]	2.36×10^{-4}[f]		2.07×10^{-4}[f]		1.75×10^{-4}[f]		
β_T (m m^{-1} %$^{-1}$)	3.30×10^{-3}[d]	9.18×10^{-4}[f]		9.14×10^{-4}[f]		9.79×10^{-4}[f]		
β_R (m m^{-1} %$^{-1}$)	2.10×10^{-3}[d]	2.86×10^{-3}[f]		3.57×10^{-3}[f]		5.00×10^{-3}[f]		$1.27 \times 10^{+10}$[j]
E (Pa)								
E_L (Pa)	$1.38 \times 10^{+10}$[e]	$6.72 \times 10^{+9}$[f]	$7.00 \times 10^{+9}$[f]	$9.50 \times 10^{+9}$[f]	$9.83 \times 10^{+9}$[f]	$1.23 \times 10^{+10}$[f]	$1.30 \times 10^{+10}$[f]	
E_T (Pa)	$6.78 \times 10^{+8}$[e]	$9.27 \times 10^{+9}$[f]	$9.84 \times 10^{+8}$[f]	$1.54 \times 10^{+9}$[f]	$1.61 \times 10^{+9}$[f]	$2.15 \times 10^{+9}$[f]	$2.21 \times 10^{+9}$[f]	
E_R (Pa) G (Pa)	$1.31 \times 10^{+9}$[e]	$7.50 \times 10^{+7}$[f]	$8.50 \times 10^{+7}$[f]	$1.26 \times 10^{+8}$[f]	$1.51 \times 10^{+8}$[f]	$1.47 \times 10^{+8}$[f]	$1.70 \times 10^{+8}$[f]	$4.72 \times 10^{+9}$[k]
G_{LR} (Pa)	$1.01 \times 10^{+9}$[e]	$1.54 \times 10^{+8}$[f]	$1.62 \times 10^{+8}$[f]	$2.24 \times 10^{+8}$[f]	$2.29 \times 10^{+8}$[f]	$2.45 \times 10^{+8}$[f]	$2.44 \times 10^{+8}$[f]	
G_{TR} (Pa)	$2.55 \times 10^{+8}$[e]	$7.70 \times 10^{+7}$[f]	$8.20 \times 10^{+7}$[f]	$1.06 \times 10^{+8}$[f]	$1.36 \times 10^{+8}$[f]	$1.24 \times 10^{+8}$[f]	$1.47 \times 10^{+8}$[f]	
G_{LT} (Pa) v	$7.53 \times 10^{+8}$[e]	$3.37 \times 10^{+9}$[g]	$1.12 \times 10^{+9}$[g]	$1.63 \times 10^{+9}$[g]	$1.99 \times 10^{+9}$[g]	$2.57 \times 10^{+9}$[g]	$2.68 \times 10^{+9}$[g]	0.35[l]
v_{LT}	0.500[e]	0.183[h]						
v_{RT}	0.820[e]	0.019[h]						
v_{TL}	0.025[e]	0.161[h]						
v_{RL}	0.044[e]	0.013[h]						
v_{TR}	0.420[e]	0.312[h]						
v_{LR}	0.460[e]	0.364[h]						

d_b basic density, d_n nominal density, D_i diffusion coefficient in the i direction, T temperature, RH relative humidity, M_0 initial moisture content, M_1 final moisture content, h convective mass transfer coefficient, β_i shrinkage coefficient in the i direction; E_i elastic modulus in the i direction; G_{ij} shear modulus in the ij plane; v_{ij} Poisson's ratio in the ij plane

[a] Jessome [10]

[b] Siau [11]

[c] Blanchet et al. [5]

[d] Goulet and Fortin [12]

[e] Bodig and Jayne [13]

[f] Experimental value

[g] Estimated value

[h] Zhu et al. [14]

[i] Belleville et al. [7]

[j] Bandrup et al. [15]

[k] Baïlon and Drolet [16]

[l] Urayama et al. [17]

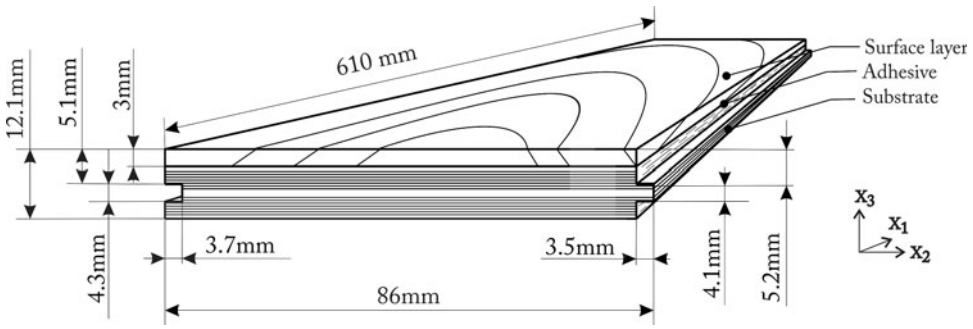

Fig. 1 Construction and geometry of EWF prototype

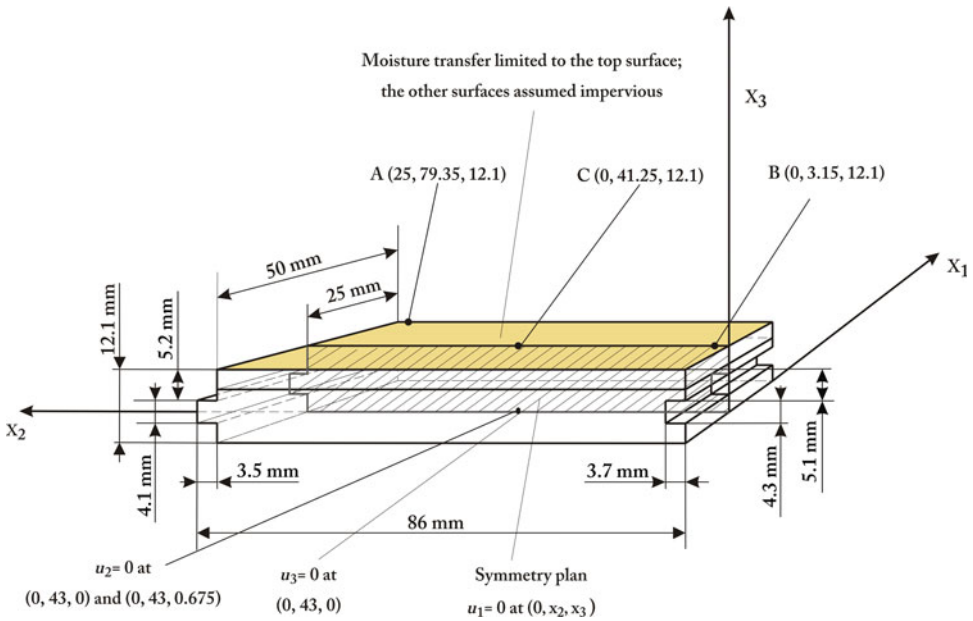

Fig. 2 Domain geometry and boundary conditions

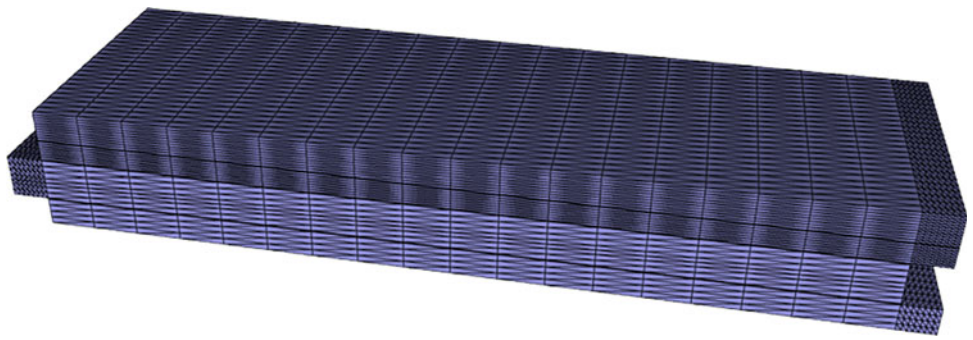

Fig. 3 Coarse finite element mesh used in the numerical model

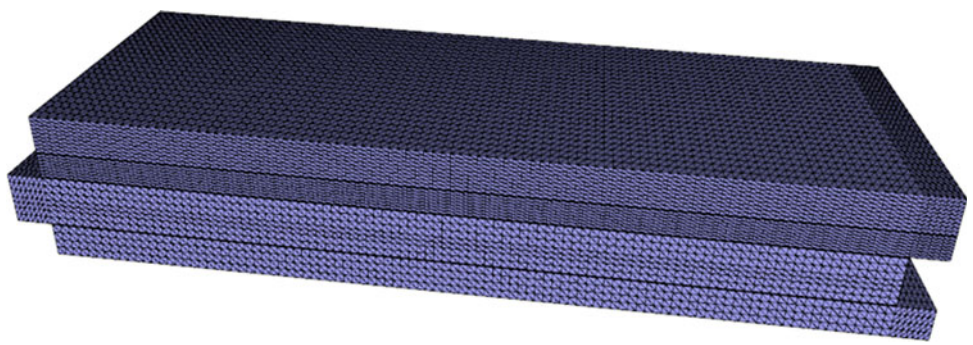

Fig. 4 Fine finite element mesh used in the numerical model

- for the surface and the adhesive layers

$$M(x_1, x_2, x_3, t_0) = M_0 = 8.6\% \quad \forall(x_1, x_2, x_3) \tag{10}$$

- for the OSB substrate

$$M(x_1, x_2, x_3, t_0) = M_0 = 6.2\% \quad \forall(x_1, x_2, x_3) \tag{11}$$

The moisture content at equilibrium was:

- for the surface and the adhesive layers

$$M(x_1, x_2, x_3, t_\infty) = M_\infty = 5.8\% \quad \forall(x_1, x_2, x_3) \tag{12}$$

- for the OSB substrate

$$M(x_1, x_2, x_3, t_\infty) = M_\infty = 3.4\% \quad \forall(x_1, x_2, x_3) \tag{13}$$

For the mechanical part of the problem, the conditions were:

Initial condition:

$$\sigma(x_1, x_2, x_3, t_0) = \sigma_0 = 0 \quad \forall(x_1, x_2, x_3) \tag{14}$$

$$u(x_1, x_2, x_3, t_0) = u_0 = 0 \quad \forall(x_1, x_2, x_3) \tag{15}$$

Boundary conditions (Fig. 2):

$$u_1 = 0 \quad \text{at } (0, x_2, x_3) \tag{16}$$

$$u_2 = 0 \quad \text{at } (0, 43, 0) \text{ and } (0, 43, 0.675) \tag{17}$$

$$u_3 = 0 \quad \text{at } (0, 43, 0) \tag{18}$$

The numerical simulations were performed using a constant time step of 0.1 s. The total time of simulation was 28 days. At each time step, the moisture content variation (ΔM) was used to calculate the corresponding displacements (u). The ΔM was also used to update the mechanical and physical properties of OSB substrate. To reduce the computation time and the data generated by the model, the mechanical calculations were realized at only 20 time steps.

To compare the simulated EWF cupping deformations with the experimental deformations, EWF prototypes were produced. The manufacturing parameters are the same as those used by Barbuta et al. [2] for EWF prototypes with an OSB substrate. After a conditioning period at 50% RH and 20°C, twelve EWF specimens of 86 mm wide and 50 mm long were placed in a conditioning room at 20% RH and 20°C for 4 weeks. Before the test in climate chamber, the EWF specimens were sealed with aluminum foil on the bottom face and the edges to impose moisture transfer by the top surface only. The cupping deformations were measured over the width of the strip with a dial gauge as described by Blanchet et al. [18]. The coordinates of measurement points (A, B, C) were introduced in the finite element model to calculate the simulated cupping deformations (Fig. 2). The cupping deformation was defined as the difference in vertical displacement between the points A and B and the central point C. The minus sign was used to indicate that the cupping is a convex deformation of the EWF strip.

Results and discussion

Engineered wood flooring cupping deformation

Figure 5 presents experimental and numerical cupping deformation as a function of time. The simulated curves from the coarse and fine meshes show a good agreement with experimental data. We note that the coarse mesh provides results closer to the experimental measurements. However, the difference between the results generated by the two meshes is small. Compared to the experimental data, the fine mesh solution overestimated the maximum deformation by 7%.

Even though the cupping simulated curve obtained from a coarse mesh is closer to the experimental one, a finer mesh is necessary for an accurate description of the interlaminar normal and shear stresses. For both experimental and numerical results (Fig. 5), approximately 91% of the maximum cupping deformation occurred in the first 10 days of the experiment. The slopes of the simulated curves in the first days are influenced by the properties of the surface layer. Blanchet et al. [5] showed that the variation of the transverse water diffusion coefficient has an important effect on the curve slope. After that period, the cupping deformation curve turns into a relatively flat plateau. It is important to indicate that the numerical simulations were performed using the mean values of the material properties without considering their variability. The average coefficients of variation (CV) for physical and mechanical properties of clear wood are between 15 and 25% [19], whereas the average measured CV values for OSB are approximately 30%. Parametric studies indicate that the maximum cupping deformation is influenced by the modulus of elasticity in parallel and perpendicular to the surface grain of OSB and by sugar maple shrinkage

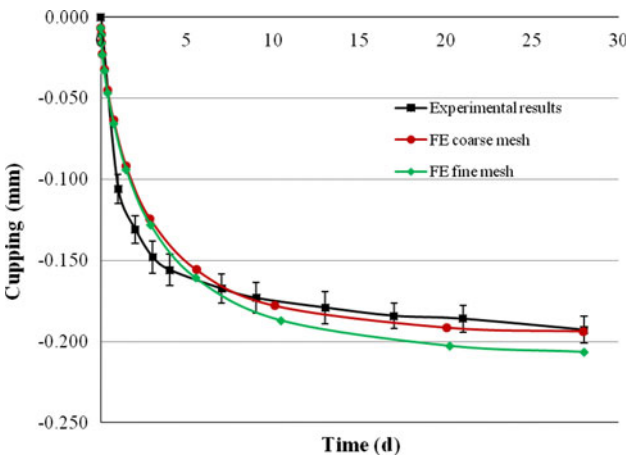

Fig. 5 Cupping deformation as function of time. Experimental and numerical results

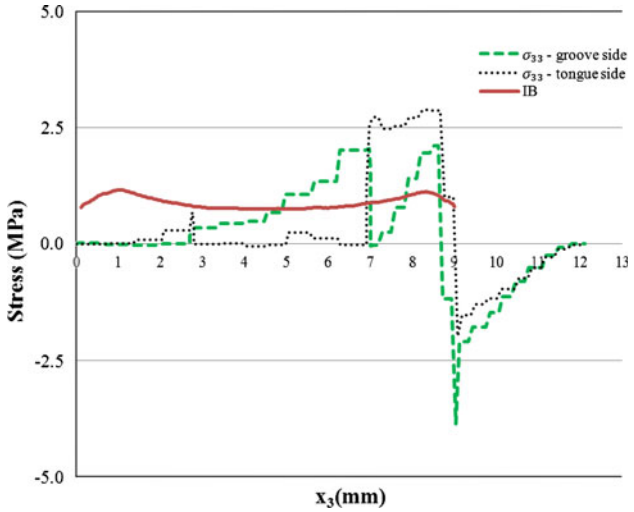

Fig. 6 Comparison between the calculated normal stress σ_{33} at the tongue and groove edges after 28 days at 20°C and 20% RH and the internal bond strength IB of the OSB substrate at 20% RH as function of x_3

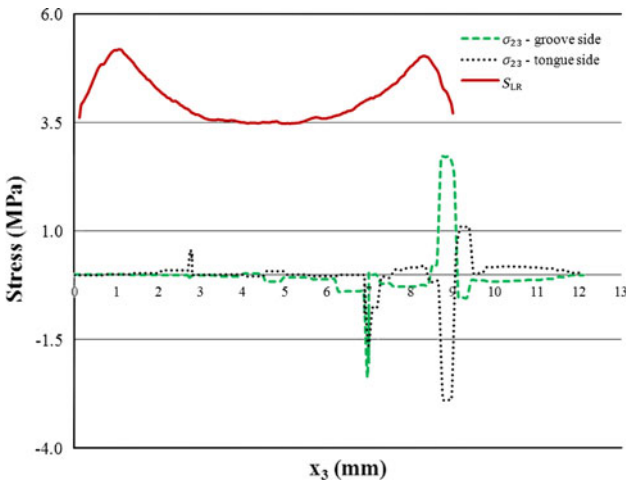

Fig. 7 Comparison between the calculated shear stress σ_{23} at the tongue and groove edges after 28 days at 20°C and 20% RH and shear strength S_{LR} of the OSB substrate at 20% RH as function of x_3

coefficient in tangential direction. The variation of these parameters with ±15% leads to a modification of the simulated maximum cupping deformation of approximately ±19%.

Stress characterization

Near the free-edges of the EWF strip, interlaminar normal and shear stresses rise sharply. These interlaminar stresses are mainly responsible for delamination fracture. In our case, the interlaminar stresses were generated by the mismatch in the shrinkage coefficients and elastic properties between the surface layer and the substrate during moisture movement. Because the shrinkage coefficient of the sugar maple surface layer is very small in the longitudinal direction (Table 1), a low level of shear stress σ_{13} is expected. The maximum of the simulated shear stress was 0.01 MPa. The distributions of interlaminar normal σ_{33} and shear σ_{23} stresses at the tongue and groove edges at $x_1 = 12$ mm, function of x_3, are presented in Figs. 6 and 7.

The two curves in each figure represent the calculated values of the stresses at the end of the 28 days experiment at 20°C and 20% RH. As we can see, the stresses σ_{33} and σ_{23} rise significantly in the OSB substrate at the vicinity of the adhesive line ($x_3 = 9$ mm). The peak normal stress σ_{33} on the tongue side is higher than that on the groove side [2.88 MPa compared to 2.11 MPa (Figs. 6, 8)]. This difference is attributed to the presence of the groove in the OSB substrate. On the groove side, another peak stress is generated at $x_3 = 7$ mm which decreases slowly to the bottom of the EWF strip. On the other side, the level of maximum stress remains relatively constant until the tongue and decreases to practically zero at $x_3 = 7$ mm. The stress peaks σ_{23} on the tongue and groove sides are opposite and relatively symmetrical with a maximum of 2.88 MPa (Figs. 7 and 8). The shear stresses decreased rapidly after only 0.3 mm. As in the case of the stress σ_{33}, the presence of the groove generates another stress peak at $x_3 = 7$ mm. A rough comparison between the simulated maximum stresses and the ultimate strength determined according to ASTM D 1037 [9] were made. The mean values of internal bond strength (IB) and shear strength (S_{LR}) as a function of density for unidirectional OSB panels with flat density profile (Table 2) were linearly extrapolated to determine the shear and internal bond strengths as a function of vertical density profile of the OSB substrate (Figs. 6, 7).

The comparison shows that only the simulated tensile stress σ_{33} is higher than the internal bond strength (Fig. 6). It seems that the model overestimates the stress field in the vicinity of the EWF strip free-edges. The use of an elastic model may explain this overestimation of the stress. Moses and Prion [20] also used an elastic finite element model to predict the strength of laminated veneer lumber (LVL). They found that shear stresses obtained from the model were approximately 1.7 times higher than nominal values.

The stress fields (Fig. 8) obtained from the model are in accordance with the observation made on the OSB samples after conditioning at 20°C and 20% RH. Seven out of twelve samples presented micro-delamination: five between the glue line and the tongue and six in the groove zone.

Figure 9 presents the distribution of the calculated normal and shear stresses at free-edges function of x_2. The maximum values at free-edges were found at $x_3 = 8.34$ mm on the

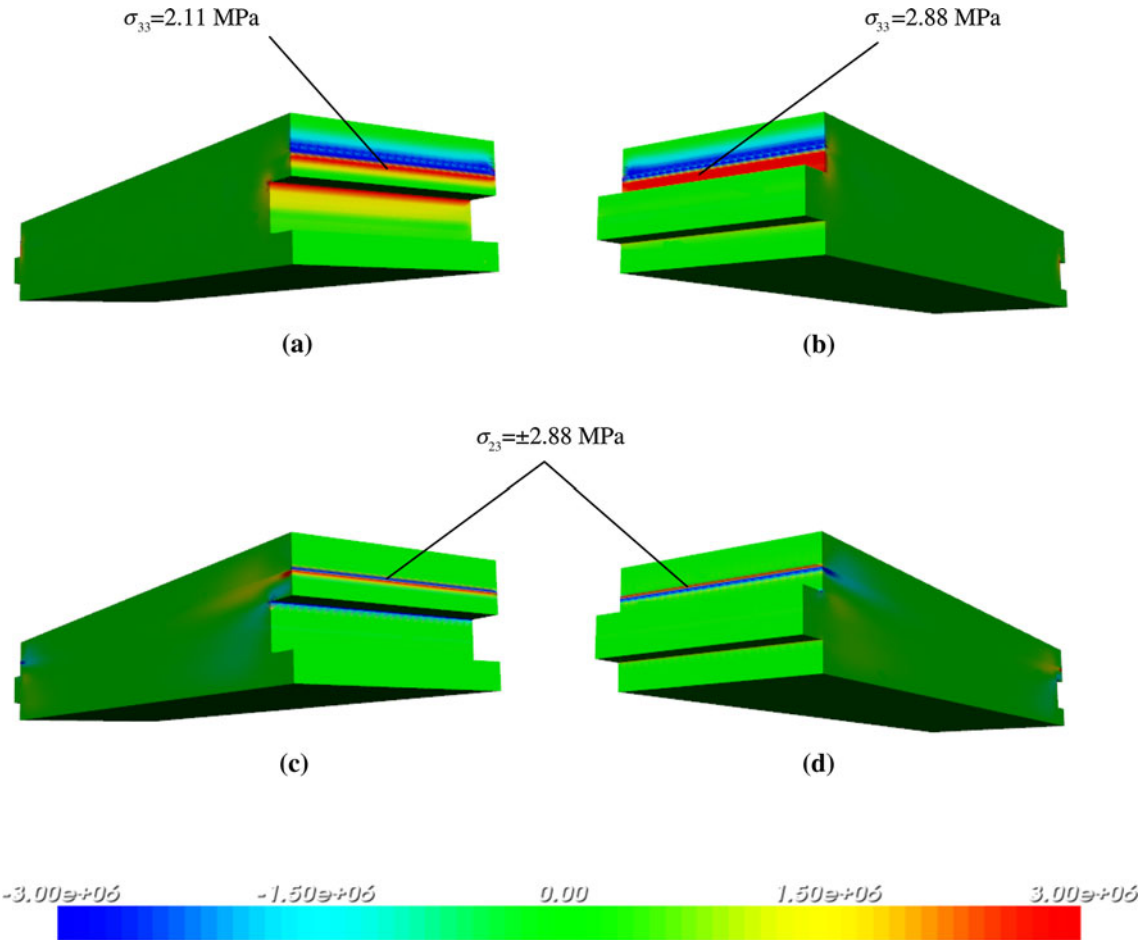

Fig. 8 Stress fields calculated by the model; **a** groove side normal stress σ_{33}; **b** tongue side normal stress σ_{33}; **c** groove side shear stress σ_{23}; **d** tongue side shear stress σ_{23}

Table 2 Internal bond strength and shear strength of unidirectional OSB with flat density profile as a function of nominal density at 20°C and 20% RH

Parameters	Unidirectional OSB nominal density		
	500 kg/m^3	650 kg/m^3	800 kg/m^3
IB (MPa)	0.583	0.829	1.054
S_{LR} (MPa)	2.714	3.898	4.708

IB internal bond strength, S_{LR} shear strength in the LR plane

tongue side and at $x_3 = 8.5$ mm on the groove side for the normal stress σ_{33} and at $x_3 = 8.8$ mm for shear stress σ_{23} on both sides (Fig. 8). As expected, the magnitude of the interlaminar normal and shear stresses increases rapidly as the free-edges are approached. This phenomenon is more evident in the case of the normal stress which reaches the maximum in approximately 0.5 mm from the free-edge. The shear stress begins to increase/decrease at about 30 mm from the free-edges. The positive or negative signs of the shear

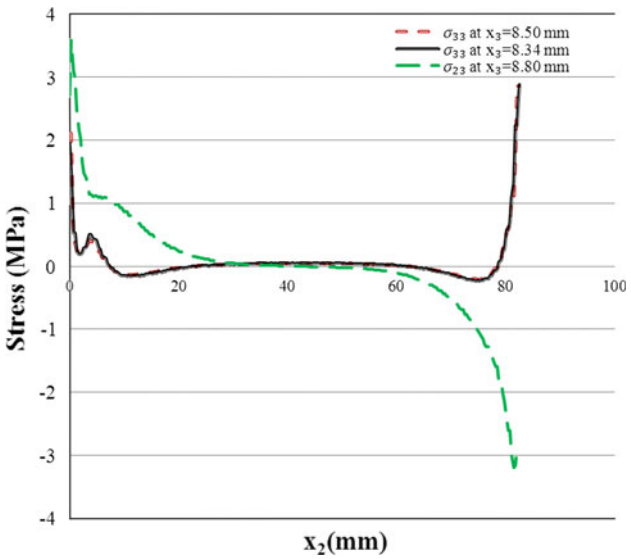

Fig. 9 Distribution of the maximum calculated normal σ_{33} and shear σ_{23} stresses at free-edges as a function of x_2

stress on the groove and tongue sides indicate that the stress acts in the positive or negative direction of the axis. These stresses are opposite to ensure the mechanical equilibrium. The non-symmetrical shapes and the difference between the maximum values on the groove and tongue sides of the stresses are due to the presence of the groove.

Conclusions

The main objective of this study was to characterize the interlaminar stress responsible for delamination at free-edges in EWF. A three-dimensional finite element model was used to predict the cupping deformation and to characterize stresses developed in the EWF. The physical and mechanical properties of the OSB substrate required in the model were determined experimentally.

Good agreement has been found between the numerical and experimental EWF cupping deformation. Compared to the experimental measurement, the finite element solution overestimates the maximum deformation by 7%. Parametric studies indicate that the maximum cupping deformation is influenced by the MOE in parallel and perpendicular directions of the OSB substrate and by the shrinkage coefficient in tangential direction of the sugar maple. The variation of these parameters with ±15% leads to a modification of the simulated maximum cupping deformation by approximately ±19%.

The stress distribution fields generated by the model are in accordance with the delaminations observed on the OSB substrate after conditioning at 20°C and 20% RH. Delamination in EWF can occur principally under the action of the tension stress or a combination of tension and shear stress. Finally, simulated results show that the levels of interlaminar stresses are the highest near the free-edges of EWF.

References

1. Barbuta C, Blanchet P, Cloutier A, Yadama V, Lowell E (2010) Tailor made OSB for special application. Eur J Wood Prod 69:511–519
2. Barbuta C, Blanchet P, Cloutier A, Yadama V, Lowell E (2010) OSB substrate for engineered wood flooring. Eur J Wood Prod 70:37–43
3. Cloutier A, Gendron G, Blanchet P, Ganev S, Beauregard R (2001) Finite element modeling of dimensional stability in layered wood composites. In: 35th international particleboard/composite materials symposium. Washington State University, Pullman, Washington, pp 63–72
4. Reddy JN (1993) An introduction to the finite element method, 2nd edn. McGraw Hill, New York, p 684
5. Blanchet P, Gendron G, Cloutier A, Beauregard R (2005) Numerical prediction of engineered wood flooring deformation. Wood and Fiber Sci 37(3):484–496
6. Blanchet P, Cloutier A, Gendron G, Beauregard R (2006) Engineered wood flooring design using the finite element method. Forest Prod J 56(5):59–65
7. Belleville B, Cloutier A, Blanchet P, Deteix J (2008) Wood-adhesive interface characterization and modeling in engineered wood flooring. Wood Fiber Sci 40(4):484–494
8. Deteix J, Blanchet P, Fortin A, Cloutier A (2008) Finite element modeling of laminate wood composites hygromechanical behavior considering diffusion effects in the adhesive layers. Wood Fiber Sci 40(1):132–143
9. ASTM International (2006) Standard methods of evaluating the properties of wood-based fiber and particle panel materials. Standard D 1037-06a. American society of testing and materials, vol 4.10
10. Jessome AP (2000) Strength and related properties of woods grown in Canada. Forintek Canada Corp. Special Publication SP514E, Canada, p 37
11. Siau JF (1995) Wood: influence of moisture on physical properties. Department of Wood Science and Forest Products. Virginia Polytechnic Institute and State University. Blacksburg, Virginia, p 227
12. Goulet M, Fortin Y (1975) Mesure du gonflement de l'érable à sucre au cours d'un cycle de sorption d'humidité à 21°C. Research note no. 12, Département d'Exploitation et Utilisation des Bois, Université Laval, Québec, p 49
13. Bodig J, Jayne BA (1993) Mechanics of wood and wood composites. Krieger Publishing Company, Malabar, p 712
14. Zhu EC, Guan Z, Rodd PD, Pope DJ (2005) Constitutive models of OSB and its application in finite element analysis. Holz Roh Werkst 63(2):87–93
15. Bandrup I, Immergut EH, Grulke EA (1999) Polymer handbook, 4th edn. John Wiley & Sons, New York, p 1904
16. Baïlon JP, Drolet JM (2000) Des Matériaux, 3rd edn. École Polytechnique de Montréal, Montréal, p 740
17. Urayama K, Takigawa T, Masuda T (1993) Poisson's ratio of polyvinyl alcohol gels. Macromolecules 26(12):3092–3096
18. Blanchet P, Beauregard R, Cloutier A, Gendron G, Lefebvre M (2003) Evaluation of various engineered wood flooring constructions. Forest Prod J 53(5):30–37
19. Wood Handbook: wood as an engineering material (2010) US Department of Agriculture, Forest Service, Forest products laboratory, p 508
20. Moses DM, Prion HGL (2002) Anisotropic plasticity and the notched wood shear block. Forest Prod J 52(6):43–54